



Construction of ratiometric fluorescence MIPs probe for selective detection of tetracycline based on passion fruit peel carbon dots and europium

Xue Sun^{1,2} · Minwen Jiang¹ · Ligang Chen¹ · Na Niu^{1,3}

Received: 28 April 2021 / Accepted: 5 July 2021 / Published online: 16 August 2021
© The Author(s), under exclusive licence to Springer-Verlag GmbH Austria, part of Springer Nature 2021

Abstract

A new type of ratiometric molecularly imprinted fluorescence probe (B-CQDs@Eu/MIPs) based on biomass carbon quantum dots (B-CQDs) and europium ions (Eu^{3+}) has been prepared to recognize and detect tetracycline (TC). In the experiment, the fluorescent material B-CQDs were prepared using passion fruit peels through microwave-assisted method, which by the meantime achieves the reuse of biomass waste. TC can block the transition of some parts of electrons in the prepared B-CQDs from the excited state to the ground state, resulting in the weakening of its blue light ($\text{Ex} = 394 \text{ nm}$, $\text{Em} = 457 \text{ nm}$), while TC can be chelated by Eu^{3+} and emit red characteristic fluorescence ($\text{Ex} = 394 \text{ nm}$, $\text{Em} = 620 \text{ nm}$) due to the antenna effect. Thus, a ratiometric fluorescence response to TC is the result of the combined B-CQD and Eu^{3+} . Based on this, we established the ratiometric fluorescent molecularly imprinted (MIP) probe for the detection of TC. The prepared B-CQDs@Eu/MIPs is aimed at catching the fluorescence changes of target tetracycline (TC) sensitively with the special combination of the specific recognition cavities and TC. The linear fluorescence quenching range of TC in milk using the fluorescent probe was 25–2000 nM, and the detection limit was 7.9 nM. The recoveries of this method for TC were 94.2–103.7%, and the relative standard deviations (RSDs) were 1.5–5.3%. Owing to the predetermined nature of MIP technology and the special response of ratio fluorescence, the interference of common substances is eliminated completely, which greatly improved the selectivity of its practical applications.

Keywords Molecular imprinted polymer · Biomass carbon quantum dots · Ratiometric fluorescence probe · Fluorescence quenching mechanism · Tetracycline

Introduction

TC is a kind of broad-spectrum antibiotic discovered in the 1940s, which is widely used in a variety of infections caused by rickettsia, chlamydia, mycoplasma, etc. [1]. TC is also commonly applied to the animal husbandry due to its good efficacy and low price. However, the continuous excessive application of TC can cause bacterial resistance and have a serious impact on organisms [2]. Therefore, the detection of TC is of great significance. By now, the most common detection techniques of TC are high-performance liquid chromatography, capillary electrophoresis, and chemiluminescence [3–5]. Although these methods exhibit good sensitivity, long detection time and large use of organic solvents are required. Hence, it is still necessary to construct a kind fast respond method, such as the fluorescence analysis.

Nanomaterials, as a kind functional material, have been widely used in various fields due to their unique small size effect [6–10]. Carbon quantum dots (CQDs), as a carbon-

Xue Sun and Minwen Jiang contributed equally to this work.

✉ Ligang Chen
analchem@nefu.edu.cn

✉ Na Niu
niuna@nefu.edu.cn

¹ College of Chemistry, Chemical Engineering and Resource Utilization, Key Laboratory of Forest Plant Ecology, Northeast Forestry University, 26 Hexing Road, Harbin 150040, China

² School of Pharmacy, Jiamusi University, 258 Xuefu Street, Jiamusi 154007, Heilongjiang, China

³ Key Laboratory of Bio-based Material Science and Technology (Ministry of Education), College of Material Science and Engineering, Northeast Forestry University, 26 Hexing Road, Harbin 150040, China

based zero-dimensional nanomaterial, have been widely synthesized by various approaches, such as one-pot hydrothermal method, microwave-assisted method, pyrolysis method, and electrochemical oxidation method [11–13]. CQDs has unique properties such as stable optical properties, good biocompatibility, low toxicity, and easy to functionalization. Therefore, CQDs have become a promising material in many fields, including chemical sensing, bio-imaging, catalysis, and optoelectronic devices [14–16]. In traditional preparation methods, citric acid or other chemicals are utilized as the carbon precursor. Recently, easily available biomass waste as the raw materials for preparing biomass carbon quantum dots (B-CQDs) has become a new idea. For example, Pooja et al. reported B-CQDs synthesized by papaya pulp with an excellent fluorescence yield of 23.7% [17]. However, the B-CQDs are in poor selectivity in some chemical sensor applications.

In recent years, as a functional polymer with specific recognition, molecularly imprinted polymers (MIPs) have been widely used in various fields [18]. One-pot synthesis MIPs are considered to be a simple strategy [19, 20]. For example, Arabi et al. reported a silica-based hydrophilic molecularly imprinted nanosphere, which was used as a dispersive adsorbent in matrix solid dispersion [21]. MIPs have been used to construct fluorescent sensors due to its high selectivity, which shows greater affinity for template molecules compared with various nanomaterials for selective applications. At present, some studies have reported the combination of fluorescent probes with MIPs. Kazemifard et al. proposed a method to prepare a fluorescent receptor using rosemary leaves as a carbon source to detect the thiabendazole [22]. In our previous work, MIPs were introduced into the sensing system based on mango peel carbon quantum dots, which showed a good response to mesotrione [23]. However, the sensitivity of single-emission fluorescent sensors is easily affected by the factors of probe concentration and environment impacts. These problems can be avoided by built-in fluorescence correction of ratiometric fluorescence sensors.

Ratiometric fluorescent probe is referred as a kind of fluorescent sensor, which is constructed using two or more different fluorescent materials, such as fluorescent dyes, rare-earth luminescent materials, and quantum dots, and thus has two or more emission wavelengths [24]. So far, fluorescent probes based on lanthanides (rare-earth luminescent materials) have received extensive attention owing to their special characteristics, including good water solubility, large Stoke displacement, and long fluorescence lifetime. For instance, Li et al. prepared a lanthanide metal organic framework for the ratiometric fluorescent detection of phosphate [25]. Lei et al. constructed a proportional fluorescence sensor using $\text{Eu}^{3+}/\text{Tb}^{3+}$ -doped nickel coordination polymer for the detection of 2,6-dipicolinic acid [26]. Therefore, it can be expected that the fluorescent properties of lanthanide could be utilized in

combination with B-CQDs to develop a kind of ratiometric fluorescent probes with strong anti-interference capability.

Herein, inspired by the above comments, we aspired to construct a novel ratiometric fluorescent molecularly imprinted sensor about tetracycline assay through incorporating B-CQDs with Eu^{3+} via a simple sol-gel method. The Eu^{3+} ions are commonly used in the doped inorganic luminescent material to emit red light. B-CQDs and Eu^{3+} were doped into silica networks through a one-pot silylation procedure, which can keep the sensitivity of ratiometric fluorescence sensor. TC can suppress the emission of the imprinted cavities surrounded by B-CQDs, meanwhile enhance the emission of the imprinted cavities stems from Eu^{3+} . The new constructed probe has the advantage of strong selectivity, high sensitivity, and self-adjusting function, which can reduce the influence of environmental factors.

Experimental

Materials and instruments

All chemicals and instruments used in this experiment are listed in the Electronic Supporting Material (ESM).

Synthesis of B-CQDs

The B-CQDs were prepared by one-step microwave pyrolysis using passion fruit peels as carbon source and have a good quantum yield (The method of measuring quantum yield is detailed in ESM). First, 2.0 g chopped passion fruit peels, 0.3 g urea (5.0 mmol), and 30 mL ultrapure water were transferred into a polytetrafluoroethylene microwave digestion tank. Then the microwave digestion tank was placed in a microwave digestion device for reaction. The reaction temperature was raised from room temperature to 200 °C within 13 min using 400 W microwave irradiation, and the reaction was maintained at 200 °C for 30 min. The brown B-CQDs solution was collected, filtered with 0.22 μm membrane, and dialyzed for 48 h through cellulose ester membrane (MWCO: 500–1000). Finally, the B-CQDs were rotary evaporated to gain solid powders for further use.

Synthesis of mesoporous molecularly imprinted polymers

Mesoporous molecularly imprinted polymers (MS/MIPs) were synthesized by sol-gel method. Briefly, TC (360 mg), hexadecyl trimethyl ammonium bromide (CTAB) (0.6 g) and high purity water (90 mL) were mixed and stirred for 20 min. Then 3-aminopropyltriethoxysilane (APTES) (0.9 mL), tetraethyl orthosilicate (3.6 mL), and NaOH (1.05 mL, 2.0 M) were added. And the reaction was kept at room

temperature for 24 h. After that, the products were collected by centrifugation at 7000 rpm for 5 min. Ethanol/HCl (2.0 M) (9:1, v/v) was used as a washing solution to extract CTAB and TC by Soxhlet extraction at 60 °C for 48 h. Finally, MS/MIPs were dried at 60 °C in vacuum for 24 h.

Synthesis of B-CQDs@Eu/MIPs

B-CQDs (15 mL, 1 mg mL⁻¹), europium (III) nitrate hexahydrate (60 mL, 20 mM), 5'-guanosine monophosphate disodium (GMP) (3.0 mL, 10 mM), MS/MIPs (5.0 g), ethanol (5.0 mL), and APTES (2.0 mL) were reacted in the dark for 24 h at room temperature. Next, the solid products were centrifuged 5 min at 6000 rpm and washed several times by ethanol and high purity water. The non-molecularly imprinted polymers, which combined Eu³⁺ and B-CQDs (B-CQDs-Eu@NIPs), were prepared through a similar approach without TC.

Detection of TC

The fluorescence spectra of the samples were recorded using an excitation wavelength at 394 nm, the excitation and emission slits width of 10 nm, and the photomultiplier of 500 V. The B-CQDs@Eu/MIPs (15 mg) were added into 15 mL of Tris-HCl buffer solution (pH = 9) for further fluorescence measurement. A certain amount (1.5 mL) of the above B-CQDs@Eu/MIPs solution was put into a 5.0 mL cuvette, and 1.5 mL of the analyte standard solutions with given concentration (25–2000 nM) was added. After vigorously mixing for 3 min, the fluorescence spectra were collected immediately. The contrast experiments of B-CQDs@Eu/NIPs were carried out through the same procedure.

Sample collection and pretreatment

The proposed method is suitable for the detection of TC in milk samples. Pretreatment is required for the use of milk samples (The detailed steps are listed in [ESM](#)).

Results and discussion

Preparation of B-CQDs@Eu/MIPs

The synthesis procedure of B-CQDs@Eu/MIPs as well as its ratiometric fluorescence analysis principle was schematically illustrated in Fig. 1. Firstly, the microwave-assisted heating method was used to synthesize fluorescent B-CQDs with passion fruit peels as carbon source. More than 50% of the composition of passion fruit peels is sugar. Sugars in the preparation process are usually dehydrated into hydroxyl methyl furfural followed by a cascade consisting of ring-opening reactions, substitutions, cycloadditions, and polycondensations to

form the final carbon structure [27]. The role of urea is to dope nitrogen during the process of synthesizing B-CQDs, so that the B-CQDs have more surface functional groups and excellent quantum yield. Meanwhile, the influences of different conditions on the synthesis process were investigated in order to gain the best fluorescent properties of the as-prepared B-CQDs. Generally, temperature is considered an important factor in the preparation of B-CQDs. It is found that (Fig. S1a) the fluorescence intensity of B-CQDs increased as the synthesis temperature increased from 140 to 200 °C. The increase of the fluorescence intensity became smaller after the temperature was higher than 200 °C. When the quality of passion fruit peels used (2.0 g) was fixed, the fluorescence intensity of B-CQDs increased with the increasing of urea quality (0–0.4 g). The fluorescence intensity tended to be flat when the urea used was more than 0.3 g (Fig. S1b). Therefore, the B-CQDs have the best fluorescence performance under the synthesis condition of heating 2.0 g of passion fruit peels and 0.3 g of urea at 200 °C. In addition, the polymerization conditions of B-CQDs@Eu/MIPs were also optimized during the experiment. Different B-CQDs@Eu/MIPs were prepared by changing the amount of template molecules (0–500 mg) and the ratio of Eu³⁺ and B-CQDs (0–0.1 mM: mg). The fluorescence response of B-CQDs@Eu/MIPs was best when the amount of template molecule is 360 mg and the ratio of Eu³⁺ and B-CQDs was 0.08 mM: mg.

Then, B-CQDs and Eu³⁺ were introduced into MS/MIPs (prepared by one-pot method) as the signal recognition unit to obtain B-CQDs@Eu/MIPs. In this procedure, APTES acts as cross-linker to connect MS/MIPs and B-CQDs. The GMP can connect both B-CQDs and Eu³⁺ to realize the introduction of these two fluorescent components. The materials are conducive to the mass transfer owing to the mesoporous molecular imprinting as a core, which has larger pores. In addition, APTES as the cross-linking agent formed a thin silicon layer, which has no prevention on mass-transfer of target analyte to imprinted cavities of MIPs. Without TC in the system, B-CQDs@Eu/MIPs emitted blue light with a strong emission at 457 nm and a weak emission at 620 nm due to the forbidden transition. When the target TC molecule entered into the interior of B-CQDs@Eu/MIPs through specific holes, it can block the transition of some parts of electrons in the B-CQDs from the excited state to the ground state, resulting in the weakening of blue light. At the meanwhile, the chelating of surface hydroxyl groups and benzene ring of TC with Eu³⁺ ions can increase the fluorescence intensity of Eu³⁺ at the wavelength of 620 nm by the antenna effect, resulting in ratiometric fluorescent response towards TC.

Characterization of materials

Figure 2a displays the TEM image of as-prepared B-CQDs showing that the B-CQDs is mostly spherical in structure and

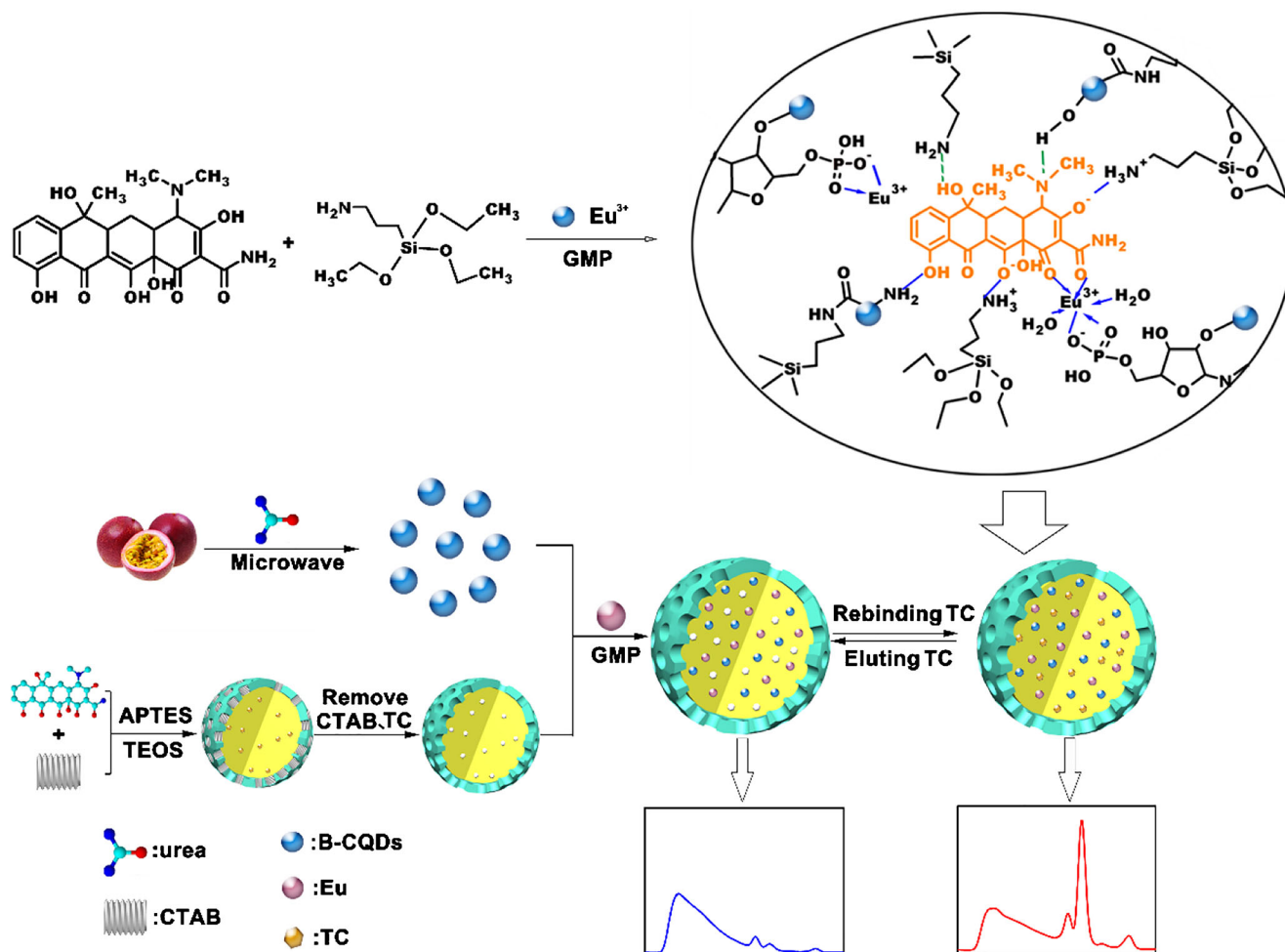


Fig. 1 Illustration of the preparation of B-CQDs@Eu/MIPs

has good dispersibility. It can be seen from the HRTEM images (inserted in Fig. 2a) that the lattice spacing of the prepared B-CQDs is 0.32 nm, which is consistent with that in the literature [28]. From a quantity of B-CQDs, we estimated that the diameter of the B-CQDs ranged from 1.7 nm to 4.2 nm (Fig. 2b). The size and shape of B-CQDs@Eu/MIPs were characterized by SEM and TEM. B-CQDs@Eu/MIPs exhibit irregular particle shape with diameter of about 180–300 nm (Fig. 2c and d).

The FTIR spectra of B-CQDs and B-CQDs@Eu/MIPs nanocomposites are shown in Fig. 3a, which revealed their characteristic of functional groups. The broad peak at 3401 cm⁻¹ of the B-CQDs FTIR spectrum may due to the stretching vibration of O-H bond and N-H bond [29]. The characteristic peak of C-O bond at 1070 cm⁻¹ is ascribed to the -OH of the B-CQDs. The peak at 1674 cm⁻¹ can be ascribed to the stretching vibration of the C=O bond of the B-CQDs. In addition, the sharp band at 1384 cm⁻¹ is due to the in-plane bending vibration of N-H, indicating the existence of -NH₂ groups on the surface of B-CQDs [30]. The surface-rich functional groups of B-CQDs were important for the further

synthesis of MIPs and its coordination with Eu³⁺ ions. For B-CQDs@Eu/MIPs, the peaks at 3401 cm⁻¹, 1570 cm⁻¹, and 1384 cm⁻¹ were weakened [31], indicating that the -OH group, -NH₂ group, and C=O group on the surface of B-CQDs have interacted with APTES and Eu³⁺ ions. The strong peak at 1049 cm⁻¹ was attributed to the Si-O-Si bond, and the peaks at 784 cm⁻¹ and 456 cm⁻¹ were ascribed to the Si-O bond, indicating the successful formation of B-CQDs@Eu/MIPs.

The X-ray diffraction (XRD) patterns of B-CQDs and B-CQDs@Eu/MIPs are shown in the Fig. 3b. B-CQDs has a broad peak around 2θ = 22°, indicating that the B-CQDs is amorphous [32]. The pattern of B-CQDs@Eu/MIPs was similar to that of the B-CQDs, except that the main peak shows a slight shift to a large angle, which possibly due to the amorphous structure formed by the enclosed organic material.

The surface elements of the as-prepared material were analyzed by X-ray photo-electron spectroscopy (XPS). The full range XPS analysis clearly showed (Fig. 3c) three peaks at 291.6, 401.2, and 533.2 eV, which were attributed to C1s, N1s, and O1s, respectively. For B-CQDs, the high-

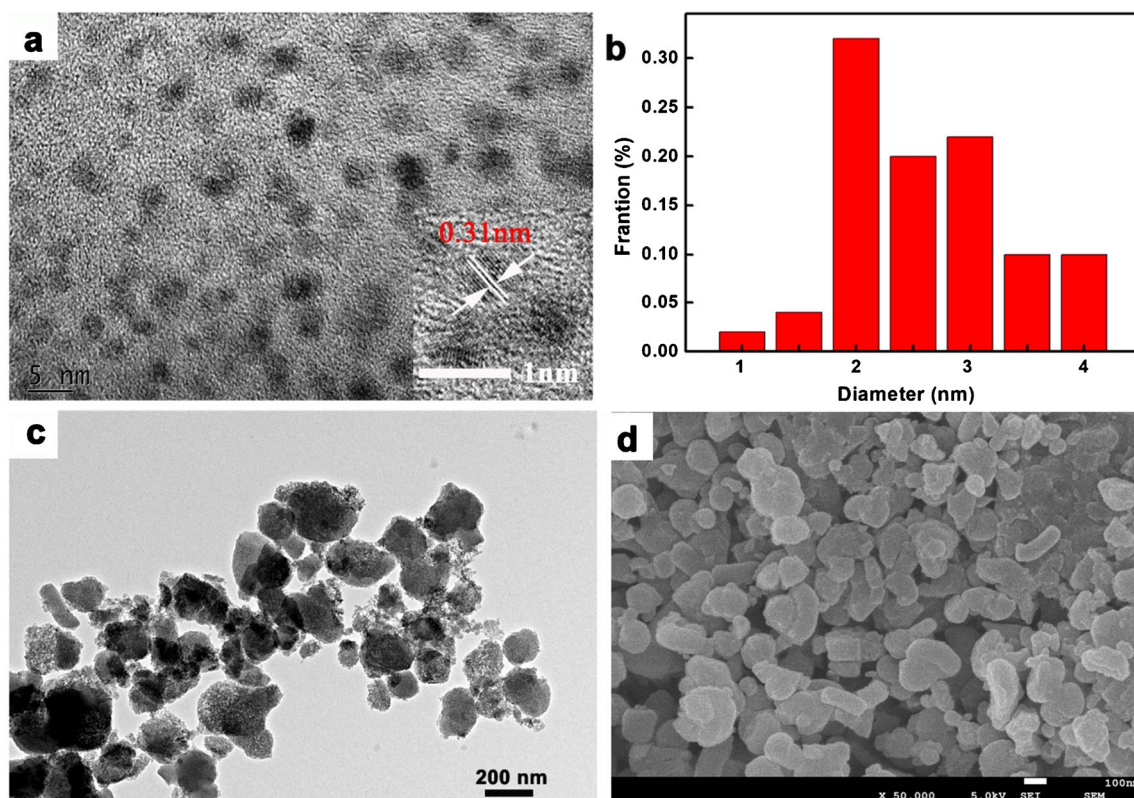


Fig. 2 TEM images and high-resolution TEM images (a), size distributions (b) of B-CQDs, TEM images (c), SEM images, and (d) of B-CQDs@Eu/MIPs

resolution XPS scan of C1s (Fig. 3d) can be split into three surface contents, that is, C-N (288.5 eV), C-O (289.5 eV), and O-C=O (291.3 eV) [33]. The high-resolution spectra of N1s (Fig. 3e) revealed the presence of both C-N and N-H bonds owing to the presence of peaks at 403.7 eV and 404.5 eV, respectively. The high-resolution XPS scan of O1s (Fig. 3f) showed three peaks at 535.5 eV, 536.4 eV, and 537.3 eV, which were attributed to C-N, C-O, and O-C=O, respectively. The XPS results were roughly consistent with the FT-IR analysis. Besides, the peak intensities of C1s, N1s, and O1s of B-CQDs@Eu/MIPs composites were weaker than B-CQDs and produced new Si2p, Si2s, and Eu3p peaks, which can be attributed to the formation of MIPs.

Optimization of the B-CQDs@Eu/MIPs

Optimization of probe concentration

The interaction between the probe and TC was affected by the using concentration of probe. It can be seen from Fig. S2a that the F_{Eu}/F_{B-CQDs} ratio increases with the increase of probe concentration when a fixed concentration of TC (2000 nM) was detected. When the concentration was higher than 1.0 mg mL^{-1} , the ratio of F_{Eu}/F_{B-CQDs} tended to be stable. When the probe concentration is high, the ratio of F_{Eu}/F_{B-CQDs} does not increase due to the self-quenching effect and

the aggregation of the probe. For the sake of economy, the selected concentration of the probe was 1.0 mg mL^{-1} .

Optimization of binding time

The influence of different binding times of TC in the B-CQDs@Eu/MIPs system on the F_{Eu}/F_{CQDs} was also explored. The experiments showed that the fluorescence intensity of Eu^{3+} increased after the addition of TC, while the fluorescence intensity of B-CQDs decreased. As demonstrated in Fig. S2b, the F_{Eu}/F_{B-CQDs} significantly increased within 3 min and then tended to a stable value. Therefore, this experiment selects the binding time of 3 min.

Optimization of pH

The pH value is a very important parameter due to its relation with the ionic form of the template molecule. For the purpose of obtaining high sensitivity for TC detection, the pH of the reaction solution was optimized. As shown in Fig. S2c, the fluorescence intensity ratio (F_{Eu}/F_{B-CQDs}) of the B-CQDs@Eu/MIPs remained steady in the pH range of 3 to 12. B-CQDs@Eu/MIPs showed the strongest fluorescence signal at pH = 9 with TC. And the fluorescence intensity ratio was decreased whether increasing or decreasing the reaction pH, indicating that the reaction was most severe under this condition. The pK_a values of

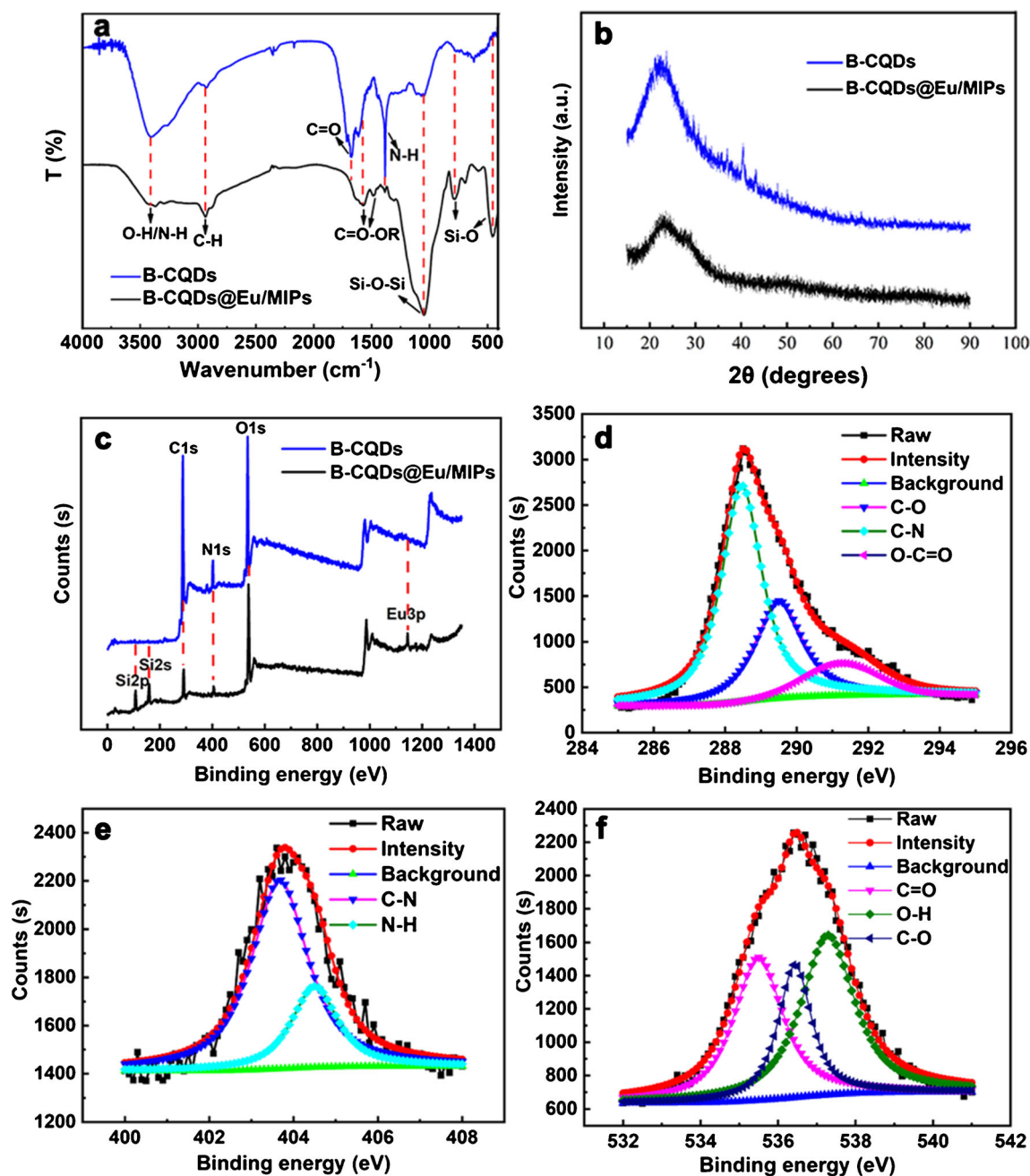


Fig. 3 FTIR spectrum (a), XRD pattern (b), XPS full survey (c) of B-CQDs and B-CQDs@Eu/MIPs, and high-resolution XPS spectra of B-CQDs@Eu/MIPs (d–f)

TC were 3.3, 7.7, and 9.7 (Fig. S3a) [34]. Due to the protonation/deprotonation procedure, at different pH values, TC molecules had different ion states, such as H_3TC^+ , H_2TC^0 , HTC^- , and TC^{2-} (Fig. S3b). The order of the proton binding ability of different TC ion morphologies was $TC^{2-} > HTC^- > H_2TC^0 > H_3TC^+$ (Fig. S4). When $pH < 9$, TC molecules existed mainly as anions state (H_3TC^+ , H_2TC^0 , and HTC^-), which had electrostatic attraction with the positive charge of APTES amino ($pK_a = 9.7$) in B-CQDs@Eu/MIPs. When $pH = 9$, TC molecules existed mainly as HTC^- (75%) and TC^{2-} (20%); thus the electrostatic attraction with APTES was the strongest. When $pH > 9$, the TC molecule

was negatively charged which electrostatically repelled the negatively charged APTES. Furthermore, Eu^{3+} can make better interaction with different ion forms of TC when the pH value in range of 3 to 12.

Tetracycline detection in sample by B-CQDs@Eu/MIPs

The matrix-matched calibration method was used during the experiment. The linear range is determined by adding a series of concentrations of tetracycline to the milk sample. Then the samples were treated by the

method described previously, and the fluorescence detection is performed. Figure 4a–b showed that the blue fluorescence of B-CQDs at 457 nm was quenched when the concentration of TC in milk sample was gradually increased from 25 to 2000 nM, whereas the red fluorescence of Eu^{3+} at 620 nm enhanced significantly. These cause the fluorescent color of the ratiometric probe gradually changed from blue to red. To investigate the fluorescence quenching efficiency of TC for B-CQDs@Eu/MIPs, the Stern-Volmer equation was used to assess the quenching efficiencies of B-CQDs@Eu/MIPs and B-CQDs@Eu/NIPs. The quenching effect of TC on B-CQDs@Eu/MIPs and B-CQDs@Eu/NIPs can be estimated using the following Stern-Volmer equation:

$$\frac{F_{\text{Eu}}}{F_{\text{B-CQDs}}} = 1 + K_{\text{SV}}C \tag{1}$$

where F_{Eu} and $F_{\text{B-CQDs}}$ are the fluorescence intensities of Eu^{3+} and B-CQDs after adding TC, respectively; C represents the concentration of TC, and K_{SV} represents the quenching constant. Obviously, it can be recognized that the fluorescence intensity ratio ($F_{\text{Eu}}/F_{\text{B-CQDs}}$) has a good linear relationship with the TC concentration (25–2000 nM). The regression equations of B-CQDs@Eu/MIPs and B-CQDs@Eu/NIPs in the liner range from 25 to 2000 nM were listed as follows: $F_{\text{Eu}}/F_{\text{B-CQDs}} = 1.49 \times 10^{-3} C + 0.5636$ (B-CQDs@Eu/MIPs) and $F_{\text{Eu}}/F_{\text{B-CQDs}} = 4.01 \times 10^{-4} C + 0.5422$ (B-CQDs@Eu/NIPs). The correlation coefficients (R^2) of above calculated equations of B-

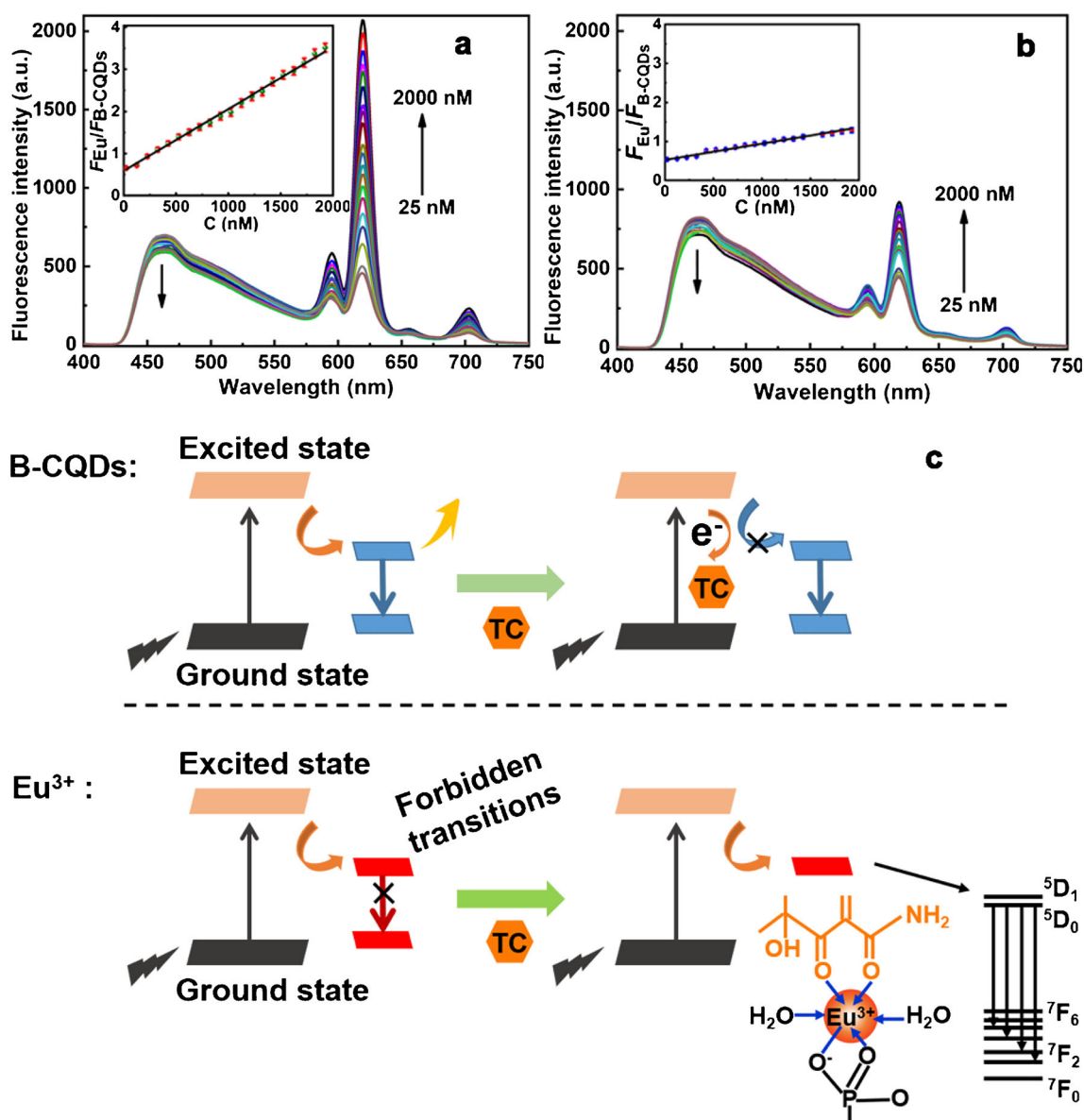


Fig. 4 Fluorescence emission spectra (Ex = 394 nm, Em = 457 nm and 620 nm) of B-CQDs@Eu/MIPs (a) and B-CQDs@Eu/NIPs (b). Schematic of the light-emitting mechanism of B-CQDs@Eu/MIPs (c)

CQDs@Eu/MIPs and B-CQDs@Eu/NIPs were 0.9966 and 0.9863, respectively. Based on the linear relationship obtained, the calculated detection limit (LOD) of TC was 7.9 nM. The LOD is obtained based on the ratio of the blank standard deviation to slope ($LOD = 3\sigma/K_{sv}$). The blank standard deviation is obtained by measuring a blank solution without adding tetracycline 10 times. The specific formula is $\sigma = \sqrt{\frac{1}{n} \sum_1^n (x_i - \bar{x})^2}$, where x is the ratio of the fluorescence intensity ($x = F_{Eu}/F_{B-CQDs}$) of B-CQDs@Eu/MIPs.

Evaluation of B-CQDs@Eu/MIPs

Evaluation of stability

The stability of the B-CQDs@Eu/MIPs was proved by an experiment of detecting TC after irradiating continuously under a UV lamp for 7 h. As shown in the Fig. S5a, the fluorescence intensity ratio (F_{Eu}/F_{CQDs}) of B-CQDs@Eu/MIPs was basically unchanged, indicating that B-CQDs@Eu/MIPs has excellent resistance to photobleaching and good stability.

Evaluation of affinity and sensitivity

The fluorescence spectrums of B-CQDs@Eu/MIPs, B-CQDs, and Eu^{3+} are shown in Fig. S5b. The affinity and sensitivity of B-CQDs@Eu/MIPs to TC are best when the same concentration of TC (2000 nM) is added. The affinity and sensitivity of Eu^{3+} to TC are relatively weak due to the forbidden transition. B-CQDs have good affinity and sensitivity to TC, but the single fluorescence emission has weak anti-interference ability. The affinity and sensitivity of B-CQDs@Eu/MIPs to TC are best due to the coordination effect between materials.

Evaluation of selectivity

For the purpose of evaluating the specific recognition ability of B-CQDs@Eu/MIPs for the detection of TC, a series of experiments under the same detection conditions were performed on different antibiotics, including chlortetracycline, oxytetracycline, erythromycin, chloramphenicol, and thiamphenicol. As shown in Fig. S5c, B-CQDs@Eu/MIPs have the highest selectivity to TC. The possible reasons of the high selectivity are described as follows: the groups at positions 4, 6, and 10 of TC produce hydrogen bonds with B-CQDs@Eu/MIPs, and the groups on 1, 2, 3, and 12, as well as the benzene ring of TC, all undergo charge transfer with B-CQDs@Eu/MIPs. The chlortetracycline has a substituent group -Cl on the benzene ring, which results in a weak charge transfer ability (Table S1). The low selectivity of B-CQDs@Eu/MIPs for oxytetracycline is mainly due to the hydroxyl group at the 5-position which forms an intramolecular hydrogen bond with the N at the 4 position (six-membered

ring structure). And erythromycin, chloramphenicol, and thiamphenicol have no effect on B-CQDs@Eu/MIPs due to the structural differences.

B-CQDs@Eu/NIPs have a fluorescent signal because B-CQDs@Eu/NIPs and B-CQDs@Eu/MIPs contain the same fluorescent components. When TC is added to the system, part of the functional groups will contact the fluorescent components to produce fluorescent response. However, the fluorescence response of NIPs is weak because NIPs cannot recognize the specific cavity of TC and cannot completely contact the fluorescent components.

Evaluation of anti-interference capability

In addition, interfering substances that may exist in the samples are also important factors that must be considered before the probe can be used in practice. It can be seen from the Table S2 that the most probable co-existing substances indicated no conspicuous interference in our probe. The above data indicated that the B-CQDs@Eu/MIPs had an excellent selectivity and anti-interference ability.

Evaluation of reusability

Regeneration and repeatability are also important factors for evaluating fluorescence probe. The probe can be eluted with ethanoacetic acid (9:1, v/v) as the eluent. It can be easily noted from Fig. S5d that the fluorescence intensity of the material does not decrease significantly as the number of cycles increases. And the fluorescence intensity can still be reached $88.7 \pm 1.8\%$ after five cycles, indicating that the B-CQDs@Eu/MIPs have excellent repeatability and application potential.

Practical application in analyzing milk sample

To evaluate the applicability of as-prepared of B-CQDs@Eu/MIPs, this probe was used to the detection of TC in several milk samples. The detectable level of TC was not found in these samples. Meanwhile, TC in these samples was detected by HPLC-MS/MS through national standard methods (see the ESM for details). The results exhibited that TC was not discovered (Fig. S6), which was consistent with our method. Moreover, this method avoids tedious pre-separation procedures and has a short detection time compared with HPLC-MS/MS. The relative standard deviations (RSDs) of intra-day and inter-day precisions were investigated using three different concentrations (50, 500, and 1500 nM) of spiked milk samples as shown in Table S3. The intra-day precisions were 1.5–4.7%, which was measured 6 times in 1 day, while the inter-day precisions were 3.2–5.3%, which were obtained by analyzing the milk samples once a day for 6 consecutive days. And the recovery values of all spiked milk samples were 94.2–103.7%.

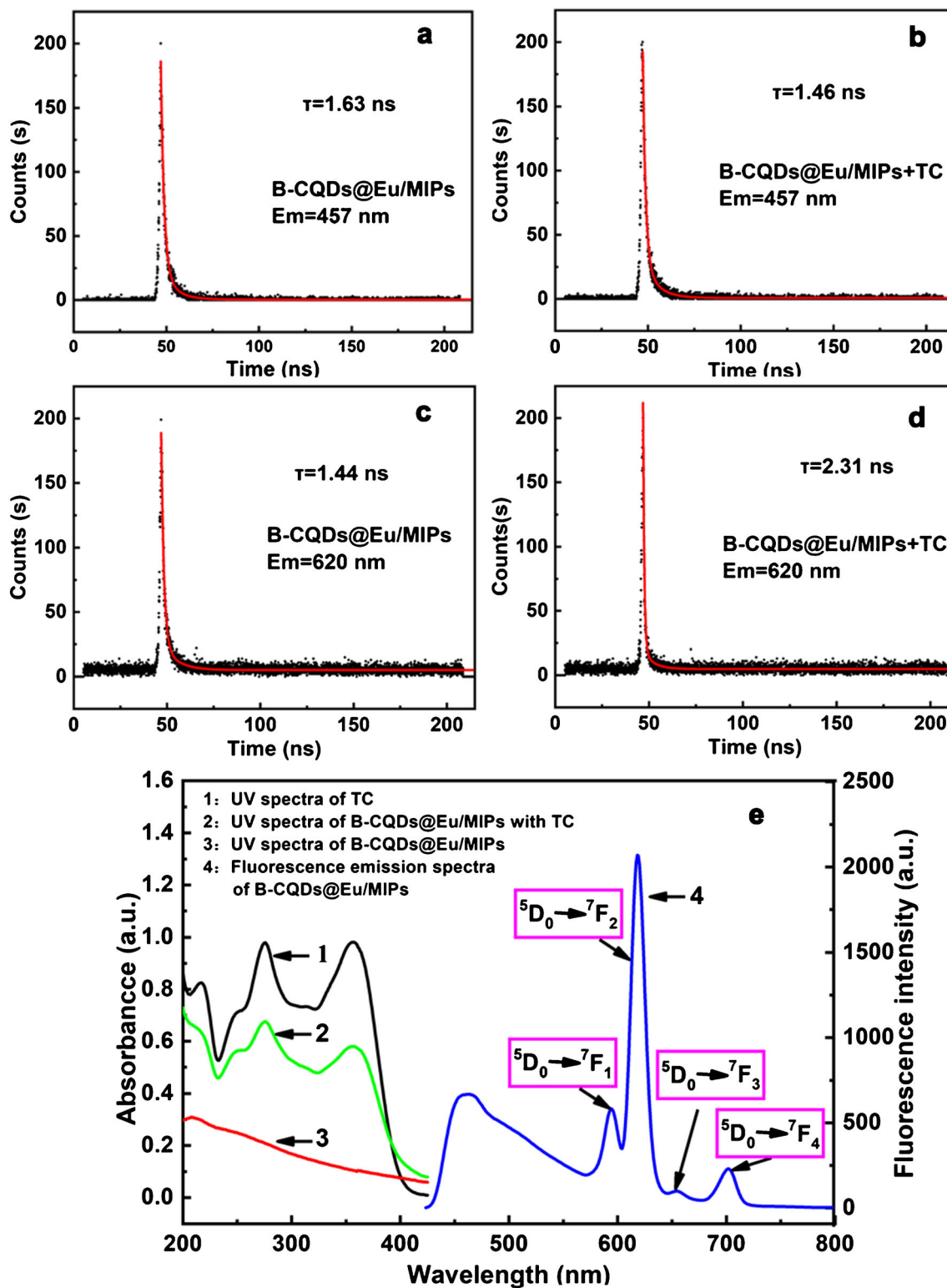


Fig. 5 Fluorescence lifetime spectra of B-CQDs@Eu/MIPs (a–d) and UV absorption and fluorescence emission combined spectrum (e)

The comparison of the analytical methods in this study with previously reported methods can be seen in Table S4. The recovery and relative standard deviation of B-CQDs@Eu/MIPs sensors were comparable to those methods. It is known

that the detection limit of B-CQDs@Eu/MIPs sensors in this study was better than several other methods except UPLC from the results. The materials of the other fluorescence methods in Table S4 are the gold nanoclusters and

functionalized metal-organic framework. The passion fruit peels have been reused in this research compared with these methods, realizing the high-value utilization of biomass waste. Moreover, the prepared B-CQDs have excellent quantum yield. Therefore, B-CQDs@Eu/MIPs are considered a new fluorescence sensor for rapid detection of TC in samples. Nevertheless, the method has the limitation of the complicated synthesis steps, which needs to simplify in the future.

Mechanism research

The mechanisms of the changing fluorescence of B-CQDs and Eu^{3+} in B-CQDs@Eu/MIPs were described in Fig. 4c. Before the addition of TC, B-CQDs@Eu/MIPs showed strong blue light emitted by B-CQDs at 457 nm. At that time, the fluorescence emission of Eu^{3+} was very weak due to the prohibition of f-f transition. When TC was added into the system, it became an effective electron acceptor. Part of the electrons in the B-CQDs were prevented to jump from the excited state back to the ground state, which results in a decrease of the blue emission from B-CQDs. In addition, the β -diketone structure on the TC will form a rare-earth organic complex with Eu^{3+} ions and transmit energy to Eu^{3+} ions through the antenna effect to make it emit its characteristic fluorescence (${}^5\text{D}_0 \rightarrow {}^7\text{F}_1$, ${}^5\text{D}_0 \rightarrow {}^7\text{F}_2$, ${}^5\text{D}_0 \rightarrow {}^7\text{F}_3$ and ${}^5\text{D}_0 \rightarrow {}^7\text{F}_4$), causing the increasing of red emission.

In general, dynamic quenching effect or static quenching effect can all quench fluorophores. The fluorescence lifetime of B-CQDs@Eu/MIPs (Fig. 5a–d) changes with the adding of TC, indicating that fluorescence quenching was dynamic quenching. Moreover, the UV absorption band of TC did not shift after the addition of B-CQDs@Eu/MIPs (Fig. 5e), which was also consistent with the phenomenon of dynamic quenching. Since TC has the broad absorption spectrum of 200–600 nm (Fig. 5e, curve 1) and does not overlap with the fluorescence emission spectrum of B-CQDs@Eu/MIPs (Fig. 5e, curve 4), the effect of TC on B-CQDs@Eu/MIPs can be most possibly considered a non-internal filtering effect.

When pH = 9, TC mostly exists as HTC^- , and the effect of TC and B-CQDs@Eu/MIPs is the strongest. The carbonyl group at the 1 and 2 positions of HTC^- forms a coordinate bond with Eu^{3+} , and the groups at the 4, 6, and 10 positions form hydrogen bonds with the B-CQDs@Eu/MIPs. There is electrostatic attraction between O^- groups at positions 3 and 12 on HTC^- and the NH_3^+ groups on APTES, so electron transfer may be the main reason that causes fluorescence quenching.

Conclusions

This study established a reliable and convenient approach to detect TC based on ratiometric fluorescence effect of the B-CQDs@Eu/MIPs. These ratiometric fluorescence sensors have

avoided environmental effects due to its built-in correction. Its utility has been established for the detection of TC in real milk samples, which has satisfying RSD and recovery rate. Although the synthesis steps of material need to be further simplified, it also provided a new consultant of the detection of TC in public food safety, which has great practical significance.

Supplementary Information The online version contains supplementary material available at <https://doi.org/10.1007/s00604-021-04929-4>.

Funding This project was funded by the Natural Science Foundation of Heilongjiang Province (B2008001), Fundamental Research Funds for the Central Universities (2572017 EB08), 111 Project (B20088), Heilongjiang Touyan Innovation Team Program (Tree Genetics and Breeding Innovation Team), Heilongjiang Postdoctoral Fund (LBH-Z16009), and China Postdoctoral Science Foundation (2016 M591501, 2017 T100218).

Declarations

Conflict of interest The authors declare that they have no competing interests.

References

1. El Hassani NEA, Baraket A, Boudjaoui S, Tenório Neto ET, Bausells J, El Bari N, Bouchikhi B, Elaissari A, Errachid A, Zine N (2019) Development and application of a novel electrochemical immunosensor for tetracycline screening in honey using a fully integrated electrochemical bio-MEMS. *Biosens Bioelectron* 130: 330–337. <https://doi.org/10.1016/j.bios.2018.09.052>
2. Wu T, Xue Q, Liu F, Zhang J, Zhou C, Cao J, Chen H (2019) Mechanistic insight into interactions between tetracycline and two iron oxide minerals with different crystal structures. *Chem Eng J* 366:577–586. <https://doi.org/10.1016/j.cej.2019.02.128>
3. Liu X, Zhang Z, Peng J, He Y (2014) High-performance liquid chromatography with resonance Rayleigh scattering detection for determining four tetracycline antibiotics. *Anal Methods* 6:9361–9366. <https://doi.org/10.1039/C4AY01747A>
4. Deng B, Xu Q, Lu H, Ye L, Wang Y (2012) Pharmacokinetics and residues of tetracycline in crucian carp muscle using capillary electrophoresis on-line coupled with electrochemiluminescence detection. *Food Chem* 134:2350–2354. <https://doi.org/10.1016/j.foodchem.2012.03.117>
5. Han SQ, Liu EB, Li H (2006) Determination of tetracycline, chlor-tetracycline and oxytetracycline by flow injection with inhibitory chemiluminescence detection using copper (II) as a probe ion. *Luminescence* 21:106–111. <https://doi.org/10.1002/bio.893>
6. Jonnalagadda M, Prasad VB, Raghu AV (2021) Synthesis of composite nanopowder through Mn doped ZnS-CdS systems and its structural, optical properties. *J Mol Struct* 1230:129875. <https://doi.org/10.1016/j.molstruc.2021.129875>
7. Mathew T, Sree RA, Aishwarya S, Kounaina K, Patil AG, Satapathy P, Hudeda SP, More SS, Muthuchelivan K, Kumar TN, Raghu AV, Reddy KR, Zameer F (2020) Graphene-based functional nanomaterials for biomedical and bioanalysis

- application. *FlatChem* 23:100184. <https://doi.org/10.1016/j.flatc.2020.100184>
8. Kannan K, Radhika D, Sadasivuni KK, Reddy KR, Raghu AV (2020) Nanostructured metal oxides and its hybrids for photocatalytic and biomedical applications. *Adv Colloid Interfac* 281:102178. <https://doi.org/10.1016/j.cis.2020.102178>
 9. Hodala JL, Moon DJ, Reddy KR, Reddy CV, Kumar TN, Ahamed MI, Raghu AV (2021) Catalyst design for maximizing C₅₊ yields during Fischer-Tropsch synthesis. *Int J Hydrogen Energ* 46:3289–3301. <https://doi.org/10.1016/j.ijhydene.2019.12.021>
 10. Basavarajappa PS, Patil SB, Ganganagappa N, Reddy KR, Ahamed MI, Raghu AV, Reddy CV (2020) Recent progress in metal-doped TiO₂, non-metal doped/codoped TiO₂ and TiO₂ nanostructured hybrids for enhanced photocatalysis. *Int J Hydrogen Energ* 45:7764–7778. <https://doi.org/10.1016/j.ijhydene.2019.07.241>
 11. Cao BM, Yuan C, Liu BH, Jiang CL, Guan GJ, Han MY (2013) Ratiometric fluorescence detection of mercuric ion based on the nanohybrid of fluorescence carbon dots and quantum dots. *Anal Chim Acta* 786:146–152. <https://doi.org/10.1016/j.aca.2013.05.015>
 12. Liu Q, Ma C, Liu XP, Wei YP, Mao CJ, Zhu JJ (2017) A novel electrochemiluminescence biosensor for the detection of microRNAs based on a DNA functionalized nitrogen doped carbon quantum dots as signal enhancers. *Biosens Bioelectron* 92:273–279. <https://doi.org/10.1016/j.bios.2017.02.027>
 13. Zhu AW, Qu Q, Shao XL, Kong B, Tian Y (2012) Carbon-dot-based dual-emission nanohybrid produces a ratiometric fluorescent sensor for in vivo imaging of cellular copper ions. *Angew Chem* 51:7185–7189. <https://doi.org/10.1002/anie.201109089>
 14. Yang WN, Zhang H, Lai JX, Peng XY, Hu YP, Gu W, Ye L (2018) Carbon dots with red-shifted photoluminescence by fluorine doping for optical bio-imaging. *Carbon* 128:78–85. <https://doi.org/10.1016/j.carbon.2017.11.069>
 15. Liu ZX, Chen BB, Liu M, Zhou H, Huang C (2017) Cu(I)-doped carbon quantum dots with zigzag edge structure for high efficient catalysis of azide-alkyne cycloadditions. *Green Chem* 19:1494–1498. <https://doi.org/10.1039/C6GC03288E>
 16. Xu HY, Zhang KN, Liu QS, Liu Y, Xie MX (2017) Visual and fluorescent detection of mercury ions by using a dually emissive ratiometric nanohybrid containing carbon dots and CdTe quantum dots. *Microchim Acta* 184:1199–1206. <https://doi.org/10.1007/s00604-017-2099-1>
 17. Rao HB, Liu W, He KQ, Zhao S, Lu ZW, Zhang SX, Sun MM, Zou P, Wang XX, Zhao QB, Wang Y, Liu T (2020) Smartphone-based fluorescence detection of Al³⁺ and H₂O based on the use of dual-emission biomass carbon dots. *ACS Sustain Chem Eng* 8:8857–8867. <https://doi.org/10.1021/acssuschemeng.0c03354>
 18. Arabi M, Ostovan A, Bagheri AR, Guo X, Wang L, Li J, Wang X, Li B, Chen L (2020) Strategies of molecular imprinting-based solid-phase extraction prior to chromatographic analysis. *TrAC Trends Anal Chem* 128:115923. <https://doi.org/10.1016/j.trac.2020.115923>
 19. Arabi M, Ostovan A, Bagheri AR, Guo X, Li J, Ma J, Chen L (2020) Hydrophilic molecularly imprinted nanospheres for the extraction of rhodamine B followed by HPLC analysis: a green approach and hazardous waste elimination. *Talanta* 215:120933. <https://doi.org/10.1016/j.talanta.2020.120933>
 20. Gholami H, Ghaedi M, Ostovan A, Arabi M, Bagheri AR (2019) Preparation of hollow porous molecularly imprinted and aluminum(III) doped silica nanospheres for extraction of the drugs valsartan and losartan prior to their quantitation by HPLC. *Microchim Acta* 186:702. <https://doi.org/10.1007/s00604-019-3794-x>
 21. Arabi M, Ostovan A, Zhang Z, Wang Y, Mei R, Fu L, Wang X, Ma J, Chen L (2021) Label-free SERS detection of Raman-inactive protein biomarkers by Raman reporter indicator: toward ultrasensitivity and universality. *Biosens Bioelectron* 174:112825. <https://doi.org/10.1016/j.bios.2020.112825>
 22. Kazemifard N, Ensafi AA, Rezaei B (2020) Green synthesized carbon dots embedded in silica molecularly imprinted polymers, characterization and application as a rapid and selective fluorimetric sensor for determination of thiabendazole in juices. *Food Chem* 310:125812. <https://doi.org/10.1016/j.foodchem.2019.125812>
 23. Sun X, Liu Y, Niu N, Chen L (2019) Synthesis of molecularly imprinted fluorescent probe based on biomass-derived carbon quantum dots for detection of mesotrione. *Anal Bioanal Chem* 411(21):5519–5530. <https://doi.org/10.1007/s00216-019-01930-y>
 24. Song YH, Chen JY, Hu DQ, Liu FF, Li P, Li HB, Chen SH, Tan HL, Wang L (2015) Ratiometric fluorescent detection of biomarkers for biological warfare agents with carbon dots chelated europium-based nanoscale coordination polymers. *Sensors Actuators B Chem* 221:586–592. <https://doi.org/10.1016/j.snb.2015.07.008>
 25. Li GY, Tong CL (2020) Dual-functional lanthanide metal organic frameworks for visual and ultrasensitive ratiometric fluorescent detection of phosphate based on aggregation-induced energy transfer. *Anal Chim Acta* 1133:11–19. <https://doi.org/10.1016/j.aca.2020.07.066>
 26. Lei H, Qi C, Chen X, Zhang T, Xu L, Liu B (2019) Ratiometric fluorescence determination of the anthrax biomarker 2,6-dipicolinic acid using a Eu³⁺/Tb³⁺-doped nickel coordination polymer. *New J Chem* 43:18259–18267. <https://doi.org/10.1039/C9NJ04501E>
 27. Thangaraja B, Solomon PR, Rangan S (2019) Synthesis of carbon quantum dots with special reference to biomass as a source - a review. *Curr Pharm Design* 25:1455–1476. <https://doi.org/10.2174/1381612825666190618154518>
 28. Lu J, Yang JX, Wang JZ, Lim AL, Wang S, Loh KP (2009) One-pot synthesis of fluorescent carbon nanoribbons, nanoparticles, and graphene by the exfoliation of graphite in ionic liquids. *ACS Nano* 3:2367–2375. <https://doi.org/10.1021/nn900546b>
 29. Raghu AV, Gadaginamath GS, Mallikarjuna NN, Aminabhavi TM (2006) Synthesis and characterization of novel Polyureas based on benzimidazolin-2-one and benzimidazolin-2-thione hard segments. *J Appl Polym Sci* 100:576–583. <https://doi.org/10.1002/app.23334>
 30. Shen LM, Chen ML, Hu LL, Chen XW, Wang JH (2013) Growth and stabilization of silver nanoparticles on carbon dots and sensing application. *Langmuir* 29:16135–16140. <https://doi.org/10.1021/la404270w>
 31. Raghu AV, Gadaginamath GS, Aminabhavi TM (2005) Synthesis and characterization of novel polyurethanes based on 1,3-bis(hydroxymethyl) benzimidazolin-2-one and 1,3-bis(hydroxymethyl) benzimidazolin-2-thione hard segments. *J Appl Polym Sci* 98:2236–2244. <https://doi.org/10.1002/app.22434>
 32. Zhu SJ, Meng QN, Wang L, Zhang JH, Song YB, Jin H, Zhang K, Sun HC, Wang HY, Yang B (2013) Highly photoluminescent carbon dots for multicolor patterning, sensors, and bioimaging. *Angew Chem Int Ed* 52:3953–3957. <https://doi.org/10.1002/anie.201300519>
 33. Wei FD, Xu GH, Wu YZ, Wang X, Yang J, Liu LP, Zhou P, Hu Q (2016) Molecularly imprinted polymers on dual-color quantum dots for simultaneous detection of norepinephrine and epinephrine. *Sensors Actuators B Chem* 229:38–46. <https://doi.org/10.1016/j.snb.2016.01.113>
 34. Wu TW, Xue Q, Liu F, Zhang J, Zhou CS, Cao JW, Chen HH (2019) Mechanistic insight into interactions between tetracycline and two iron oxide minerals with different crystal structures. *Chem Eng J* 366:577–586. <https://doi.org/10.1016/j.cej.2019.02.128>